Photochemistry and Photobiology, 2017, 93: 1259–1268

Synthesis, Photophysics and PDT Evaluation of Mono-, Di-, Tri- and Hexa-PEG Chlorins for Pointsource Photodynamic Therapy

Tobias Bornhütter[1], Ashwini A. Ghogare[2,3], Annegret Preuß[1], Alexander Greer[2,3]* and Beate Röder[1]*

[1]Department of Physics, Humboldt-Universität zu Berlin, Berlin, Germany
[2]Department of Chemistry, Brooklyn College, Brooklyn, NY
[3]Ph.D. Program in Chemistry, The Graduate Center of the City University of New York, New York City, NY

Received 19 January 2017, accepted 6 March 2017, DOI: 10.1111/php.12773

ABSTRACT

Pointsource photodynamic therapy (PSPDT) is a newly developed fiber optic method aimed at the delivery of photosensitizer, light and oxygen to a diseased site. Because of a need for developing photosensitizers with desirable properties for PSPDT, we have carried out a synthetic, photophysical and phototoxicity study on a series of PEGylated sensitizers. Chlorin and pheophorbide sensitizers were readily amenable to our synthetic PEGylation strategy to reach triPEG and hexaPEG galloyl pheophorbides and mono-, di-, triPEG chlorins. On screening these PEG sensitizers, we found that increasing the number of PEG groups, except for hexaPEGylation, increases phototoxicity. We found that three PEG groups but not less or more were optimal. Of the series tested, a triPEG gallyol pheophorbide and a triPEG chlorin were the most efficient at generating singlet oxygen, and produced the highest phototoxicity and lowest dark toxicity to Jurkat cells. A detailed kinetic analysis of the PEGylated sensitizers in solution and cell culture and media is also presented. The data provide us with steps in the development of PSPDT to add to the PDT tools we have in general.

INTRODUCTION

Pointsource photodynamic therapy (PSPDT) is a promising approach for topical applications of photodynamic therapy (Fig. 1) (1–3). It is a method of delivering photosensitizer, oxygen and light directly to the region of treatment. It consists of a hollow optic fiber delivering light and oxygen to a porous silica cap. Photosensitizer molecules are attached to the cap via a photocleavable linker. When light is applied, the photosensitized singlet oxygen initiates cleavage reactions liberating the photosensitizer molecules. To be independent of the local oxygen concentration, oxygen can be flushed through the hollow fiber. This method of treatment provides high local confinement of photosensitizer location.

The use of pheophorbide-*a* leads to a high hydrophobicity of the photosensitizer once it is cleaved from the fiber tip. In aqueous environment, like open tissue, an adherence of the photosensitizer on the fiber tip is inevitable. This needs further steps in testing and device construction in PSPDT. To improve the local distribution and minimize adherence of the photosensitizer on the fiber tip after its release, we synthesized and characterized six water-soluble photosensitizers for their potential use on the fiber tip for PSPDT.

Thus, the objective of this study was to synthesize and evaluate the performance of several water-soluble PEGylated sensitizers. We have synthesized and evaluated six sensitizers for their use *in vitro* with Jurkat cells. Fig. 2 shows the sensitizers: triPEG galloyl pheophorbide acid **1**, triPEG galloyl pheophorbide **2**, hexaPEG galloyl pheophorbide **3** and mono-, di-, triPEG chlorins **4-6**. Here, we hypothesized that adjusting the number of PEG substituents from low to high will reveal some superior ones. We have tested our hypothesis with an investigation of photophysics and Jurkat cell photokilling activity.

The new sensitizers **1-6** vary the number of PEG groups incorporated into pheophorbide-*a* or chlorin e_6 conjugates (Fig. 2). Previous work (4) has examined PEGylated chlorin e_6 photosensitizers, which were studied for hydrolytic stability, conformational flexibility, solubility and ovarian OVCAR-5 cancer cell phototoxicity. However, expanding on the PEGylation series in chlorins and pheophorbides for improved photophysical characteristics in **1-6** and in the Jurkat cancer cell line seemed worthwhile with respect to PDT evaluation to add to the tools we have for PSPDT in general.

MATERIALS AND METHODS

General information. Pyropheophorbide-*a*, chlorin e_6, mTHPC (Foscan®), *N*-(3-dimethylaminopropyl)-*N*′-ethylcarbodiimide hydrochloride (EDC), *N, N*-dimethyl-4-aminopyridine (DMAP), tri(ethylene glycol) monomethyl ether (MW = 164.20), methyl 3,4,5-trihydroxybenzoate (methyl gallate), potassium carbonate (K_2CO_3), lithium aluminum hydride ($LiAlH_4$), sodium hydroxide (NaOH), 30% HBr/AcOH, *p*-toluenesulfonic acid (*p*-TsCl), Triton X-100, methanol, ethanol, dichloromethane, tetrahydrofuran (THF), chloroform-*d* and chloroform were purchased commercially from Sigma-Aldrich or Fluka Biochemika. Synthesized products were purified by column chromatography using flash silica gel 200–400 mesh particle size. 1D and 2D NMR data were acquired on Bruker DPX400 MHz NMR instrument. HPLC data were obtained on a PerkinElmer 200 series instrument equipped with a bondclone 10 C_{18} column at 254 nm. UV–vis spectra were collected on a Hitachi U-2001 instrument. High-resolution mass spectrometry (HRMS) data were collected on an Agilent iFunnel 6550 Q-ToF LC/MS system.

*Synthesis of triPEG galloyl pheophorbide acid (**1**).* Compound **1** was synthesized from triPEG galloyl **7** and pyropheophorbide-*a* methylester in 2 steps as reported in literature (5). Briefly, pyropheophorbide-*a* methylester was reacted with 30% HBr/AcOH (1.0 mL) followed by

*Corresponding authors' emails: roeder@physik.hu-berlin.de (Beate Röder) and agreer@brooklyn.cuny.edu (Alexander Greer)
© 2017 The American Society of Photobiology

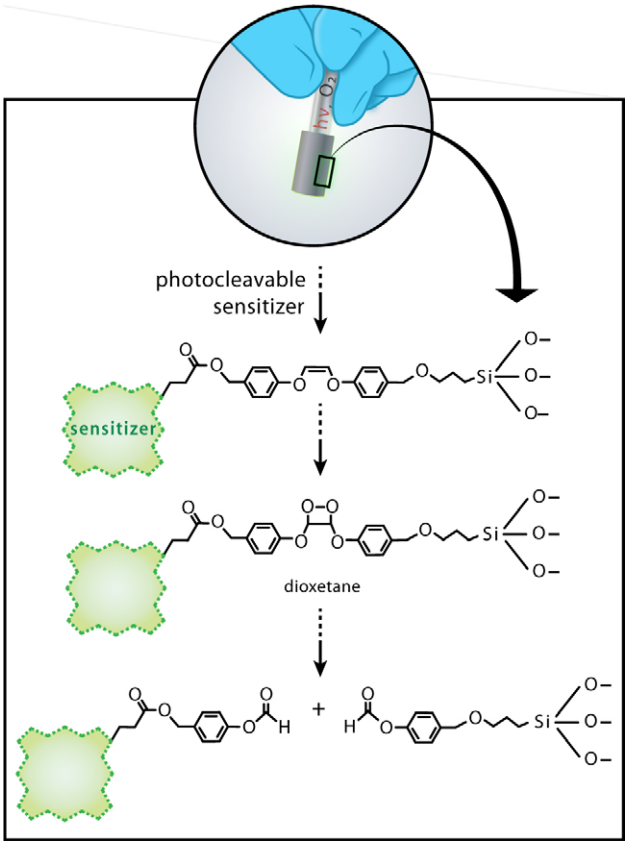

Figure 1. The concept of pointsource photodynamic therapy (PSPDT) for the delivery of sensitizer, oxygen and light (and hence singlet oxygen) to a particular biological site via a hand-held implement.

reaction galloyl-triPEG **7** and K_2CO_3 in anhydrous dichloromethane to form triPEG galloyl pheophorbide methylester. The ester was hydrolyzed in tetrahydrofuran and methanol using K_2CO_3 to form triPEG galloyl pheophorbide carboxylic acid **1** in 40% overall yield (41.0 mg, 0.036 mmol) and over 99% purity. UV−vis ($CHCl_3$): λ_{max} = 411 nm and 664 nm.

*Synthesis of triPEG pheophorbide benzyl ester (**2**).* Pyropheophorbide-*a* (20.3 mg, 0.038 mmol) dissolved in 10 mL anhydrous dichloromethane was added 64.2 mg (0.108 mmol) of triPEG galloyl **7**, 9.16 mg (0.072 mmol) of DMAP and 20.2 mg (0.108 mmol) of EDC under N_2 atmosphere. The reaction was stirred overnight at room temperature. Upon completion of the reaction, solvent was removed under vacuum and the residue obtained was chromatographed on a silica column, eluted with 5% (v/v) methanol in dichloromethane to obtain **2** in 51% yield (20.0 mg, 0.018 mmol) and 97% purity. HPLC: t_R = 19.24 min in 5% (v/v) water in acetonitrile solvent system. ^{1}H NMR (400 MHz, $CDCl_3$) δ (ppm): 9.41 (d, J = 1.2 Hz, 1H), 9.30 (s, 1H), 8.54 (s, 1H), 7.96 (dd, J = 17.8, 11.6 Hz, 1H), 6.51 (s, 2H), 6.32–6.08 (m, 2H), 5.32–5.02 (m, 2H), 5.02–4.86 (m, 2H), 4.57–4.40 (m, 1H), 4.35–4.25 (m, 1H), 4.14–4.01 (m, 6H), 3.83–3.29 (m, 47H), 3.23–3.12 (m, 3H), 2.88–2.51 (m, 1H), 2.44–2.15 (m, 1H), 1.81 (d, J = 7.3 Hz, 3H), 1.67 (t, J = 7.6 Hz, 3H), 0.39 (s, 1H), −1.75 (s, 1H). ^{13}C NMR (101 MHz, $CDCl_3$) δ (ppm): 195.91, 172.83, 171.77, 152.66, 144.66, 141.83, 138.44, 137.92, 136.47, 136.25, 132.02, 131.05, 130.73, 129.11, 122.94, 108.19, 104.07, 97.16, 72.28, 71.94, 71.90, 70.70, 70.67, 70.64, 70.51, 70.48, 69.66, 68.85, 66.56, 51.86, 50.07, 48.15, 31.12, 29.80, 23.21, 19.50, 17.33, 12.19, 12.16, 11.22. UV−vis ($CHCl_3$): λ_{max} = 411 nm and 664 nm.

*Synthesis of hexaPEG galloyl pheophorbide (**3**).* To 41.0 mg (0.036 mmol), triPEG galloyl pheophorbide acid **1** in 10 mL anhydrous dichloromethane was added 64.2 mg (0.108 mmol) of triPEG galloyl **7**, 9.16 mg (0.072 mmol) of DMAP and 20.2 mg (0.108 mmol) of EDC under N_2 atmosphere. The reaction was stirred overnight at room temperature. Upon completion of the reaction, solvent was removed under vacuum and the residue obtained was chromatographed on a silica column, eluted with 5% (v/v) methanol in dichloromethane to obtain **3** in 52% yield (30.7 mg, 0.018 mmol) and 98% purity. HPLC: t_R = 8.58 and 9.55 min (2 diastereomers of **3**) in 5% (v/v) water in acetonitrile solvent system. ^{1}H NMR (400 MHz, $CDCl_3$) δ (ppm): [9.73 (d, J = 30.5 Hz, 1H), 9.55 (s, 1H) are either meso 5-H or 10-H], 8.59 (d, J = 3.0 Hz, 1H), 6.62–6.51 (m, 4H), 6.01 (dd, J = 14.1, 6.9 Hz, 1H), 5.39–5.08 (m, 2H), 4.99 (dd, J = 8.9, 6.7 Hz, 2H), 4.68 (d, J = 11.7 Hz, 1H), 4.52 (td, J = 11.7, 9.9, 4.5 Hz, 2H), 4.40–4.28 (m, 1H), 4.21–4.06 (m, 8H), 4.04–3.27 (m, 90H), 3.18 (d, J = 2.7 Hz, 3H), 2.72 (dddd, J = 34.4, 19.4, 8.0, 4.9 Hz, 2H), 2.50–2.26 (m, 2H), 2.18 (d, J = 6.6 Hz, 3H), 1.84 (dd, J = 7.3, 2.2 Hz, 3H), 1.73 (t, J = 7.6 Hz, 3H), 0.42 (s, 1H), −1.72 (s, 1H). ^{13}C NMR (101 MHz, $CDCl_3$) δ (ppm): 196.06, 172.82, 171.38, 160.40, 160.35, 155.06, 155.01, 152.69, 152.67, 150.92, 148.96, 144.99, 141.27, 141.17, 138.76, 138.70, 138.51, 137.91, 137.84, 136.34, 136.30, 135.41, 133.72, 132.79, 132.75, 131.08, 131.05, 130.56, 128.43, 108.27, 107.60, 106.06, 104.10, 98.06, 97.76, 92.80, 72.30, 71.97, 71.93, 71.90, 71.85, 70.76, 70.71, 70.65, 70.56, 70.51, 70.48, 70.45, 69.68, 69.59, 68.90, 68.66, 66.57, 59.03, 59.00, 58.97, 51.70, 50.00, 48.08, 31.19, 31.10, 29.92, 24.62, 24.51, 23.21, 19.50, 17.52, 12.10, 11.28, 11.22, 11.16. UV−vis ($CHCl_3$): λ_{max} = 415 nm and 668 nm.

*Synthesis of triPEG galloyl (**7**).* Compound **7** was synthesized from diethylene glycol monomethyl ether and methyl gallate in three steps using a modified literature procedure (6). Briefly, triethylene glycol monomethyl ether **4** was reacted with *p*-TsCl in the presence of NaOH in THF to form PEG tosylate **5,** which was further reacted with methyl gallate **6** in the presence of K_2CO_3 in acetone to form PEGyled methyl gallate of **7**. The ester group in **7** was reduced with $LiAlH_4$ in THF to form triPEG galloyl alcohol **8** in 58% yield.

Singlet oxygen measurements. Singlet oxygen kinetics were measured using a TCMPC 1270 singlet oxygen luminescence detection system (SHB Analytics, Germany) with a frequency doubled Nd:YAG Laser (Coherent, Germany) and a self-developed dye laser as excitation source. The measurements were performed with 10 ns excitation pulses with a pulse energy of 365 nJ at 650 nm. Kinetics data were acquired from 10 measurements of 5-s integration time per measurement. The TCMPC 1270 was configured with a bandpass filter with 1270 nm center wavelength and 20 ns channel width. A bi-exponential kinetic model was fitted to determine rise and decay time, and the amplitude of the singlet oxygen luminescence kinetics (7,8) for the measurements of the pheophorbide-*a* conjugates (**1**-**3**) in aqueous solution and cells and for the measurements of the chlorin e_6 conjugates (**4**-**6**) in aqueous solution.

Singlet oxygen luminescence kinetics generated by the chlorin e_6 conjugates (**4**-**6**) in cell suspension were analyzed using target analysis methods as described in (9,10). A sequential compartment model as described in detail in (9) was used to describe the singlet oxygen luminescence kinetics generated by the chlorin e_6 conjugates (**4**-**6**) in cell suspension. The model consists of two compartments with a transfer efficiency of one from the first, the source compartment, to the second compartment and a concentration matrix containing a stretched exponential decay for the source compartment (representing the photosensitizer) and an exponential decay for the sink compartment (representing singlet oxygen).

Singlet oxygen measurements were carried out in aqueous solution and in Jurkat cells. For the measurements of the singlet oxygen generation properties in aqueous solution, the sensitizers were diluted in H_2O with 1% Triton X-100 (Fluka Biochemika) and 1% ethanol (Sigma-Aldrich) to an optical density of 0.06 at 532 nm. Singlet oxygen luminescence was measured for 10 s with excitation pulses of 160 nJ at 532 nm. All other parameters were alike to the above mentioned. For the measurements in cells, a 10-mL Jurkat cell suspension was incubated with the photosensitizers as described below and washed (400 g, 3 min) with PBS (Biochrom) two times to remove all extracellular photosensitizers. Following, the cell pellet was suspended in 5 mL PBS and given into two cuvettes (cubic, 10 mm, Sarstedt AG, Germany). Until the measurements were started, the cell suspension was kept under subdued light.

Flash photolysis measurements. To assign the rise and decay time of the singlet oxygen luminescence kinetics to the singlet oxygen lifetime and the sensitizer's triplet lifetime, latter was determined independently using laser flash photolysis. The setup consists of a 420–2500 nm laser (EKSPLA, pulse width 4–6 ns) as pump light and a stabilized 488 nm LED as probe light. The samples were excited at 650 nm, and transient

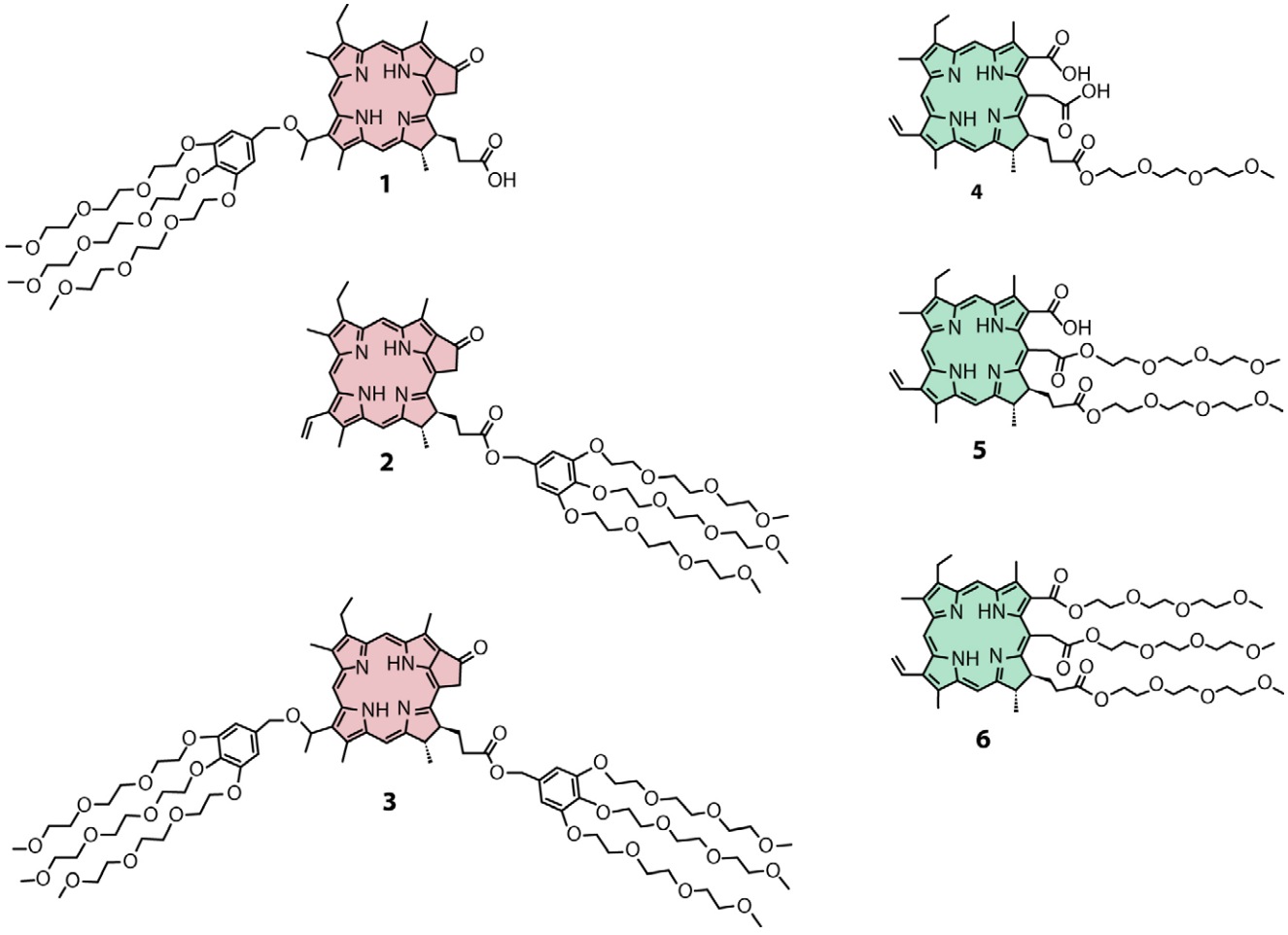

Figure 2. Structures of the PEGylated sensitizers are shown: triPEG galloyl pheophorbide acid **1**, triPEG pheophorbide benzyl ester **2**, hexaPEG galloyl pheophorbide **3** and mono-, di-, and triPEG chlorins **4**-**6**.

absorption from the lowest triplet state (triplet–triplet absorption) was detected using a 490 ± 10 nm interference filter and a Si-photodiode with an integrated fast differential pre-amplifier (Elektronik Manufaktur Mahlsdorf). The resulting signal was digitized by an oscilloscope (PicoScope 2208B, Pico Technology). This setup allows the determination of triplet lifetimes down to 0.1 μs.

Cell culture and incubation conditions. The Jurkat cells (clone E 6-1 human acute T-cell leukemia) were grown in RPMI 1640 medium with L-glutamine supplemented with 10% fetal calf serum (FCS), 100 U mL^{-1} of penicillin and 100 μg mL^{-1} of streptomycin without phenol red (Biochrom). The cells are cultivated at 37°C in 100% humidity and 5% CO_2 and are seeded in new cell culture medium every 2 or 3 days. For *in vitro* studies, the cells were incubated with 3 μM of sensitizer in the cell culture medium under subdued light for 4 h.

Phototoxicity and dark toxicity tests. The dark and phototoxicity test was prepared on 96-well plates. A 100-μL Jurkat cell suspension (~1 000 000 cells mL^{-1}) was seeded in each well and left in the incubator for 24 h. After this 24 h, the cells were incubated with additional 100-μL cell culture medium containing the different photosensitizers as mentioned above. The clinical approved photosensitizer mTHPC (Foscan®, biolitec) was used as positive control. As a blank control, the cell suspension was incubated with 0.3% ethanol, as ethanol was introduced due to the use of sensitizer stock solutions in ethanol. Each 96-well plate was prepared with 10 wells of each of the 6 photosensitizers, 10 wells with the reference and 10 wells with the positive control. The remaining 16 wells were used as empty value, which means 200 μL of cell culture medium without cells. After 4 h of incubation, the cells were illuminated with white light LEDs (~300 mJ cm^{-3}, 3 min). For the dark toxicity test, the cells were incubated under the same conditions, without illumination. After illumination, the cells were incubated in darkness, 37°C, 5% CO_2, for additional 24 h. Afterward, the viability of the cells was measured by Alamar Blue test using a plate reader (Victor3, HP) for the measurement of the resorufin fluorescence.

RESULTS AND DISCUSSION

Sensitizer synthesis

Six polyethylene glycol pheophorbide-*a* and chlorin e_6 (**1**-**6**) compounds were synthesized (note that "PEG" refers specifically to a single, monodisperse methoxytriethylene glycol group). Two of the sensitizers (**2** and **3**) are new, and their synthesis is described here. The synthesis of the other four sensitizers (**1**, **4**-**6**) has been reported previously (4,5). Our synthesis led to **1** in 40%, **2** in 51%, **3** in 52%, **4** in 50%, **5** in 48% and **6** in 33% overall yields. Based on HPLC data, the purity of **1** was 99%, of **2** was 97%, of **3** was 98%, of **4** was 95%, of **5** was 99% and of **6** was 99%.

TriPEG galloyl pheophorbide **2** and hexaPEG galloyl pheophorbide **3** were synthesized as shown in Schemes 1 and 2. Using a previously reported procedure (6,11,12), triPEG galloyl **7** was synthesized in 58% in a three-step process from triethylene glycol monomethyl ether and methyl gallate. Scheme 1 shows the condensation reaction of pyropheophorbide-*a* with

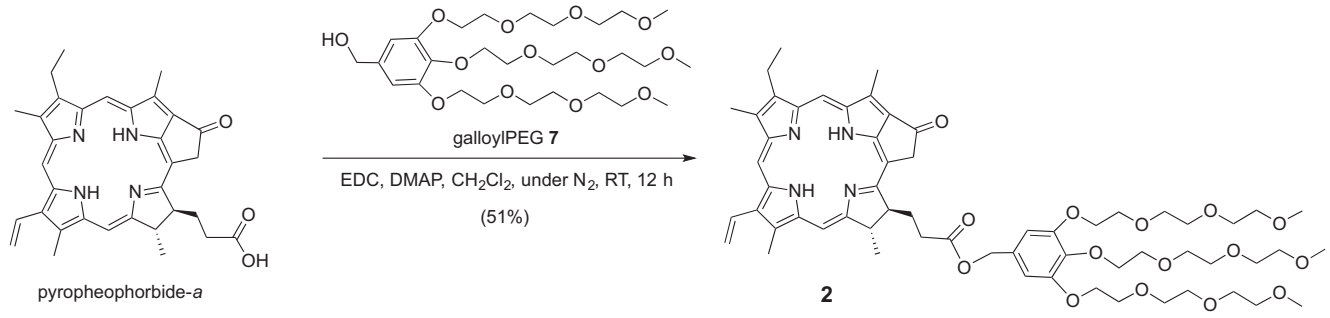

Scheme 1. Synthesis of triPEG pheophorbide benzyl ester **2**.

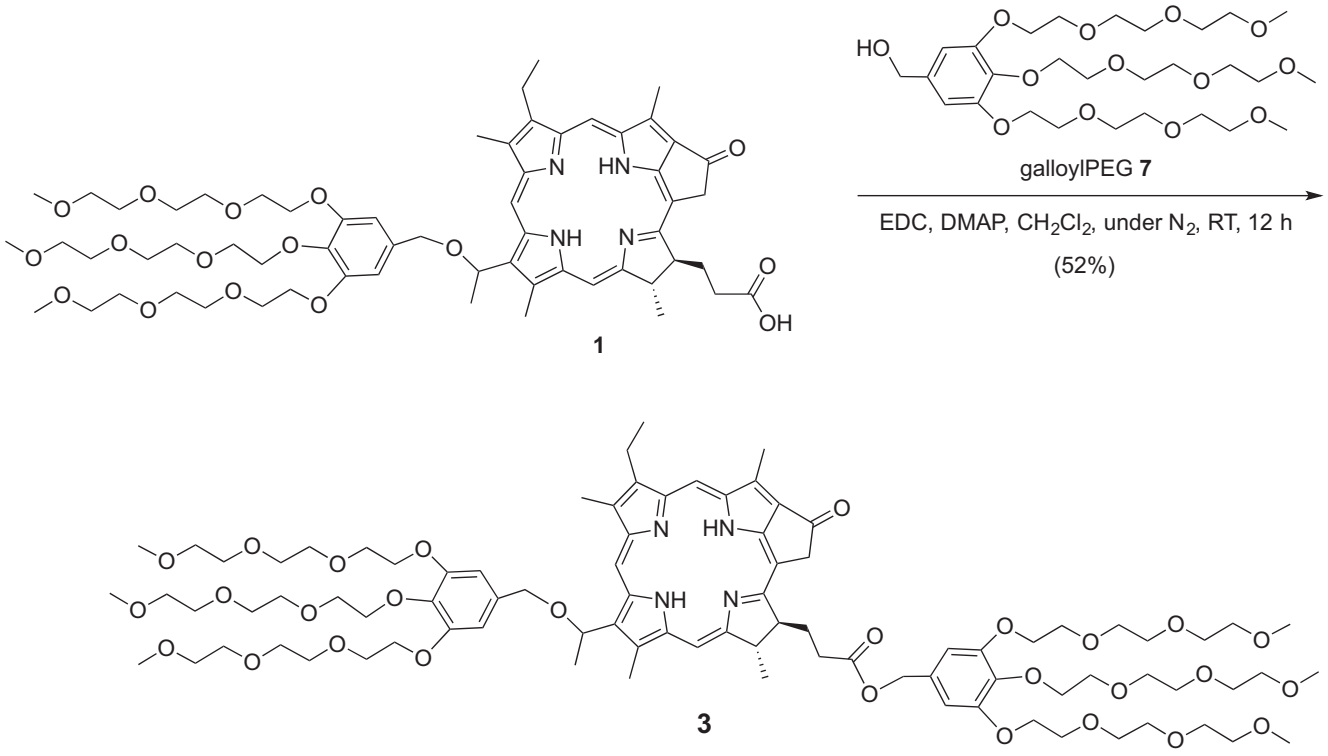

Scheme 2. Synthesis of hexaPEG galloyl pheophorbide **3**.

triPEG galloyl **7** in the presence of EDC and DMAP to form triPEG pheophorbide benzyl ester **2**. Figure 3 (upper spectrum) shows the ^{1}H NMR spectrum of **2**. For **2**, a portion of the HMBC spectra are shown in Figure S5 (Supporting Information) where three sets of signals detected for the 17^3 (172.8 ppm) carbonyl carbon coupled to protons attached to the 17^1 (2.31 ppm), 17^2 (2.65 ppm) and benzylic PEG 17^4 (4.95 ppm) carbons, suggesting an ester linkage between the 17^3 carbonyl carbon of PPa and PEG group.

Scheme 2 shows the condensation reaction of triPEG ether pheophorbide acid **1** with triPEG galloyl **7** in the presence of EDC and DMAP to form hexaPEG galloyl pheophorbide **3**. Figure 3 (lower spectrum) shows the ^{1}H NMR spectrum of **3**. For **3**, we believe an epimerization of 3^1-H causes a splitting of the meso hydrogens (5-H, 10-H and 20-H) because **3** are diastereomers. This splitting is evident in some cases, for example 9.73 (d, J = 30.5 Hz, 1H), but less resolved in other cases, for example 9.55 (s, 1H) and 8.59 (d, J = 3.0 Hz, 1H) presumably due to overlapping peaks. Also for **3**, a portion of the HMBC spectrum in Figure S11 (Supporting Information) shows three sets of signals detected for the 3^3 (70.7 ppm) carbonyl carbon coupled to protons attached to the 3^1 (6.01 ppm) and aromatic PEG (6.55 ppm) carbons, suggesting a linkage between the 3^1 alkyl carbon and one PEG group thought the ether bond. Also, portion of the HMBC spectrum shows correlation 17^3 (172.8 ppm) carbonyl carbon coupled to protons attached to the 17^1 (2.65 ppm), 17^2 (2.3 ppm) and benzylic PEG 17^4 (4.97 ppm) carbons, suggesting a linkage between the 17^3 carbonyl carbon of PPa and another PEG group through ester bond. COSY spectra for **3** showed correlation between the newly formed peak for 3^2-proton at 2.29 ppm and 3^1-protons at 6.01 ppm.

Photophysical investigations

To investigate the capability of **1**-**6** as photosensitizers, the singlet oxygen luminescence was detected in aqueous solution and

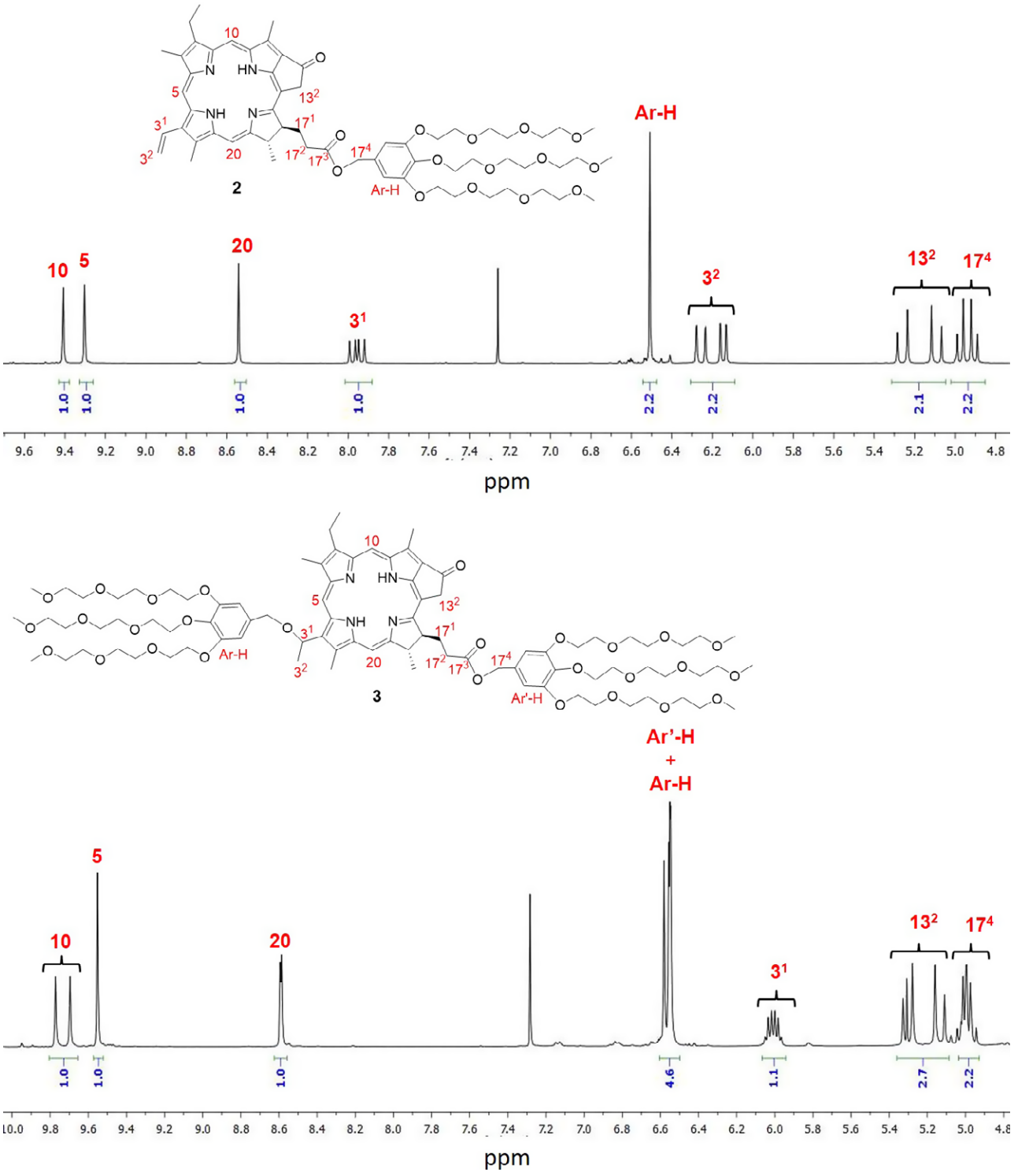

Figure 3. ^{1}H NMR spectrum of **2** (upper spectrum). ^{1}H NMR spectrum of **3** (lower spectrum) with the appearance of 4 aromatic protons between 6.5 and 6.6 ppm from both galloyl PEG groups with the 3^{1} protons at 6.01 ppm and a disappearance of alkene 3^{2} protons from (6.2 ppm), in comparison with **2**. We attribute the splitting of the meso 5, 10 and 20-H's to the two diastereomers of **3**.

in Jurkat cell suspensions *in vitro*. Figure 4 shows the time-resolved luminescence of singlet oxygen in aqueous solution and Jurkat cell suspensions generated by photosensitizers **1**-**6**. The lifetime data are shown in Table 1. In Jurkat cells, the singlet oxygen luminescence kinetics by the chlorin e_6 conjugates **4**-**6** were more complex than the pheophorbide-*a* conjugates **1**-**3**, as is discussed below.

In aqueous solution, the singlet oxygen lifetime (τ_{Δ}) of **1**-**6** is 3.5 μs (mean value) and the triplet lifetime (τ_{T}) is 2.2 μs with only slight deviation.

In Jurkat cells incubated with pheophorbide-*a* conjugates, **1**-**3** singlet oxygen lifetimes of about 3.5 µs with negligible changes of the triplet lifetimes have been observed. However, with chlorin e_6 conjugates **4**-**6** in cells, complex singlet oxygen luminescence kinetics were observed, which cannot be described by a bi-exponential kinetics model (7,8,13–15). The bi-exponential model describes the singlet oxygen luminescence kinetics of one species of photosensitizer in a homogeneous microenvironment. A deviation from this model indicates at least one of the two following scenarios: (1) There is more than one species of photosensitizer, or (2) the photosensitizer's microenvironment is inhomogeneous on a scale of tenth of nanoseconds (16).

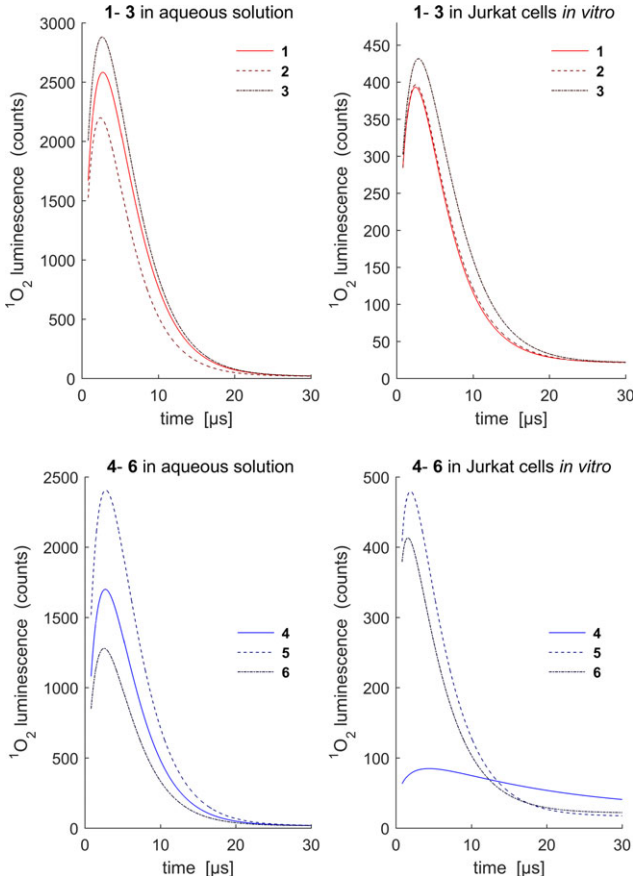

Figure 4. Singlet oxygen luminescence generated by PEGylated pheophorbides **1**-**3** and chlorins **4**-**6** in aqueous solution and in cells.

Additional experiments were carried out on chlorin e_6 conjugates **4**-**6** to probe why there was deviation from the bi-exponential model. A first step was the investigation of **4**-**6** in all cell media components involved in the cell experiments.

Figure 5 shows the kinetics of the singlet oxygen luminescence generated by chlorin e_6 conjugate **4** in cell culture medium and in water. The singlet oxygen luminescence kinetics in water follow the bi-exponential kinetics model as expected. In contrast to the singlet oxygen luminescence kinetics in water, the kinetics in cell culture medium could not be fitted bi-exponentially, but shows complex kinetics, very similar to the kinetics in cell suspensions. Photosensitizers **1**-**6** were diluted in cell culture medium for incubation of the Jurkat cells. We reason the origin of the complex singlet oxygen luminescence kinetics in cells is due to a change of the photosensitizers properties in cell culture medium.

As a next step, absorption spectra were recorded in order to find possible changes due to, for example, aggregation. Figure 6 shows the absorption spectra of chlorin e_6 conjugate **4** in water and in cell culture medium. Only negligible changes can be observed, hence no indication of aggregation of photosensitizer molecules can be observed. As aggregation of the photosensitizer

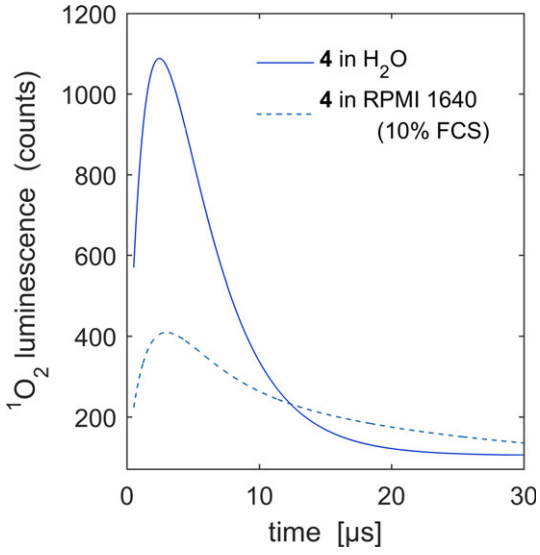

Figure 5. Singlet oxygen luminescence in water and in complete Roswell Park Memorial Institute (RPMI) 1640 media generated by **4**. In cell culture medium is an obvious change in kinetics compared to water. [Color figure can be viewed at wileyonlinelibrary.com]

Table 1. Effect of PEG group substitution on pheophorbide and chlorin on the singlet oxygen lifetime and triplet lifetime of **1**-**6** in aqueous solution and cell suspension.

	Aqueous solution*		Cell suspension*			
Compound	τ_Δ [µs]	τ_T [µs]	τ_Δ [µs]	τ_T [µs]	$\beta^\dagger$	$\tau_{T,FL}$ [µs]‡
1	3.57 ± 0.04	2.32 ± 0.03	3.85 ± 0.08	1.84 ± 0.08	–	1.84 ± 0.05
2	3.53 ± 0.03	1.89 ± 0.03	4.04 ± 0.07	1.81 ± 0.07	–	1.80 ± 0.04
3	3.49 ± 0.05	2.46 ± 0.04	3.5 ± 0.3	2.9 ± 0.3	–	2.73 ± 0.06
4	3.52 ± 0.04	2.22 ± 0.04	1.7 ± 0.4	16.9 ± 0.89	0.7	14 ± 1
5	3.58 ± 0.04	2.29 ± 0.03	4.14 ± 0.09	2.3 ± 0.2	0.8	2.37 ± 0.07
6	3.62 ± 0.04	1.95 ± 0.04	4.20 ± 0.06	1.5 ± 0.3	0.7	1.6 ± 0.1

*Deviation equates 95% confidence interval of the fit. †Identical β values were used for evaluating both, singlet oxygen luminescence kinetics and flash photolysis data. ‡Obtained from flash photolysis measurement.

is unlikely, an interaction of the photosensitizer with at least one compound of the cell culture medium appears evident.

In prior investigations, a shielding of another photosensitizer (meta-tetra(hydroxy-phenyl)-chlorin) by human serum albumin was found (17–19). In those studies, the albumins-shielded photosensitizer was taken up by the cells and was released inside Jurkat cells after an incubation time of 24 h (17–19).

Due to the albumins various binding sites for hydrophobic compounds such as hydrophobic cavities (20,21), the probability of interaction of the photosensitizers with albumins is very high (17–19,21–24). Hence, the albumins are able to shield the photosensitizer molecules and prevent its interaction with oxygen (17, 23,24). The shielding of the photosensitizer molecules by albumins does not necessarily led to a change in its absorption spectrum. Because the cell culture medium contains 10 % FCS, it is most probable that the singlet oxygen generation properties are changed due to the interaction of the photosensitizer with albumin. Unfortunately, we are unable to perform comparative experiments in the absence of FCS, as FCS is vital for the cells used in this study.

A shielding of the photosensitizer by albumins would change the oxygen accessibility to the photosensitizer. As oxygen quenching is the dominant deactivation process of the photosensitizers triplet state, a change of the oxygen accessibility would lead to a change of the photosensitizers triplet-state depletion. A shielding of the photosensitizer would also involve a change of its microenvironment, leading to a change in the singlet oxygen deactivation kinetics.

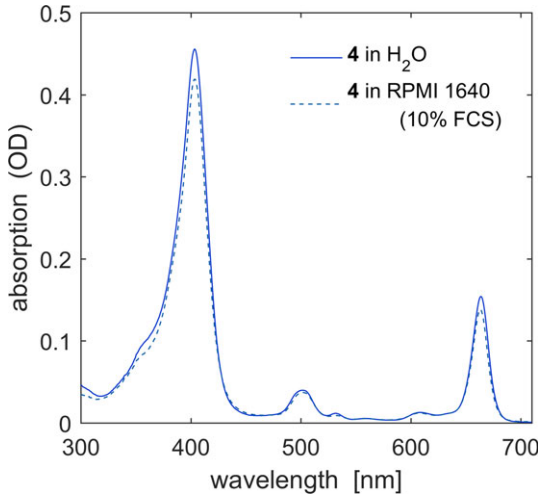

Figure 6. Absorption spectra of chlorin **4** in H_2O cell culture medium. Only negligible changes between H_2O and cell culture medium can be observed. [Color figure can be viewed at wileyonlinelibrary.com]

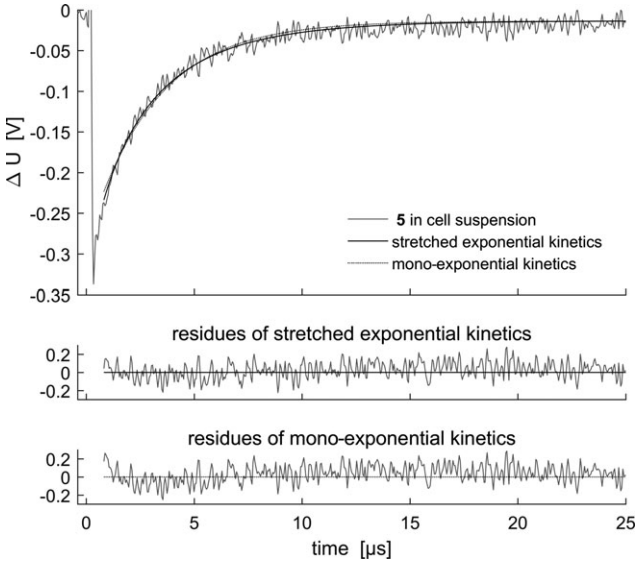

Figure 7. Flash photolysis signal of **5** in cell suspension. The residues show that a mono-exponential kinetics model do not fit the data.

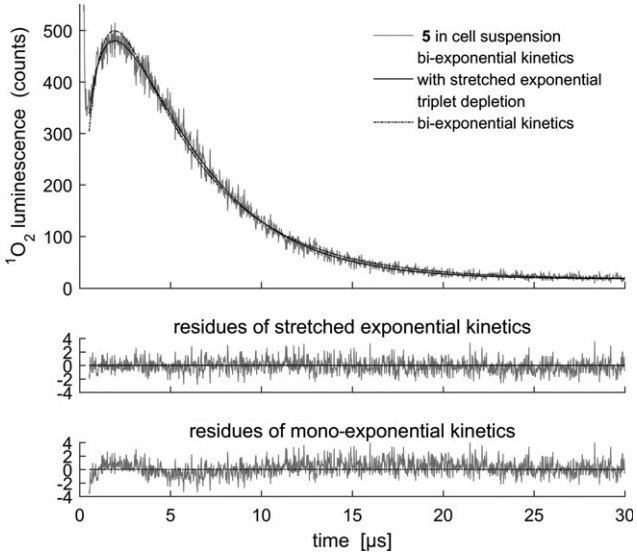

Figure 8. Singlet oxygen luminescence kinetics of **5** in cell suspension. The residues show the necessity of a stretched exponential kinetics for the depletion of the photosensitizer's triplet state.

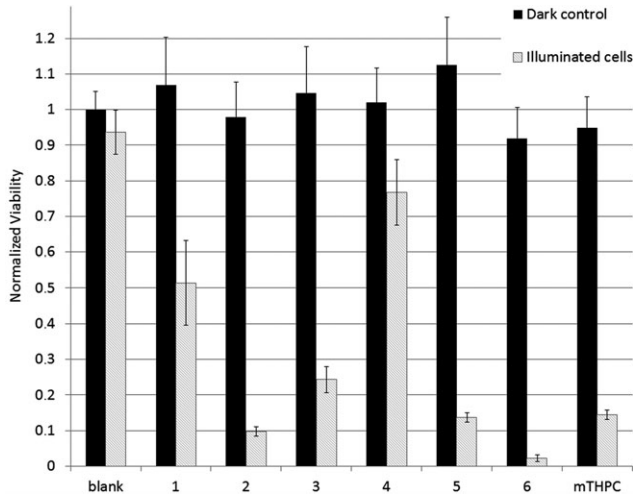

Figure 9. Dark and phototoxicity effects on Jurkat cells treated with 3 µM sensitizers **1-6** irradiated by white light LEDs (~300 mJ cm^{-2}, 3 min) after 4-h incubation. The blank contains 0.3% ethanol to check for its influence on the cells. mTHPC was used as positive control. The viability of cells was measured by a resazurin fluorescence assay. Data are normalized to the resorufin fluorescence of the reference dark toxicity experiment. The error bars represent the mean ± standard deviation of 40 samples (n = 40).

The singlet oxygen luminescence kinetics includes both, photosensitizer triplet depletion (triplet lifetime) and singlet oxygen deactivation (singlet oxygen lifetime). An inherent property of the kinetics of singlet oxygen is that it cannot be differentiated from the other without additional information. Even in a homogeneous environment, an assignment of rise and decay time of the luminescence kinetics on its own to the lifetimes of the photosensitizer's triplet state and the oxygen's singlet state is not possible (7,8,16). For that reason, the triplet-state depletion kinetics was investigated separately using laser flash photolysis. For measuring the triplet-state depletion in absence of oxygen, it was shown in (17) that gently flushing a cell solution with nitrogen in darkness leads to a substitution of oxygen by nitrogen, without killing the cells.

That is why the triplet-state depletion kinetics of chlorin e_6 conjugate **4**-**6** in cells was further investigated by laser flash photolysis as a next step. The samples were gently flushed with nitrogen for one hour in darkness. Before and after nitrogen flushing, singlet oxygen luminescence kinetics and laser flash photolysis measurements were performed.

It was found that the depletion of the triplet state of the chlorin e_6 conjugates **4**-**6** in all experiments, both flash photolysis and singlet oxygen luminescence measurement, is more complex and cannot be described by a mono-exponential decay. However, it can be described by a stretched exponential decay kinetics, using a Kohlrausch function

$$I(t) = \exp\left(-\left(\frac{t}{\tau}\right)^{\beta}\right)$$

as described in (25). This is exemplified in Fig**.** 7 by the flash photolysis signal of chlorin e_6 conjugate **5** in cells in the presence of oxygen and in Fig**.** 8 by the corresponding singlet oxygen luminescence signal. The Kohlrausch function is an empirical function that considers a distribution of depletion kinetics of the molecules' triplet state by introducing an empirical stretching parameter β with $0 < \beta \leq 1$, which corresponds to the distribution of rate constants (25–27).

Measurements after flushing the samples with nitrogen deliver matching results; that is, singlet oxygen luminescence vanishes

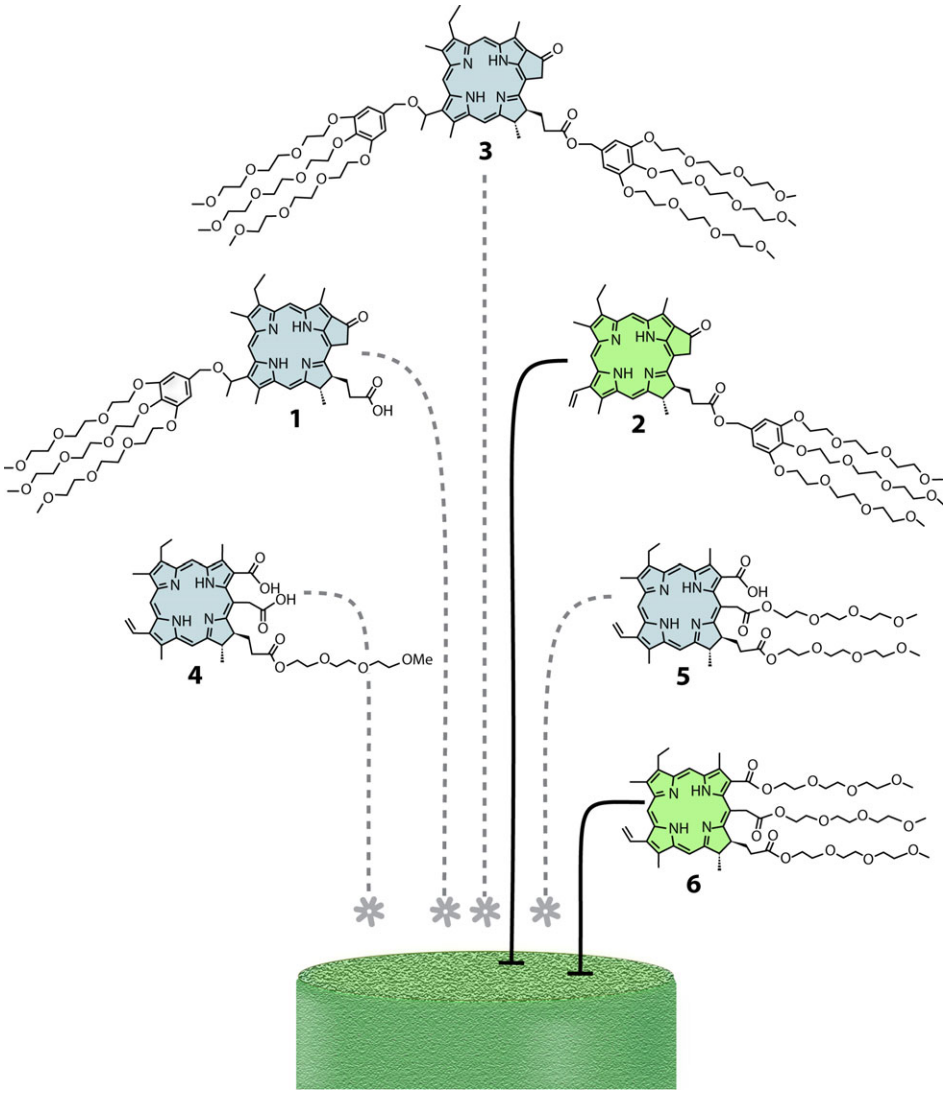

Figure 10. Image of PEGylated sensitizers in which **2** and **6** are most promising for covalent attachment to probe tips for PSPDT because of good τ_Δ and τ_T values in aqueous solution and in cell suspension, and high phototoxicity and low dark toxicity to Jurkat cells.

and flash photolysis brings a transient absorption signal, which cannot be described mono-exponential but only with a stretched exponential kinetics, revealing a triplet lifetime of about 300 μs for all chlorin e_6 conjugates. Data analysis of both, singlet oxygen luminescence kinetics and triplet-state depletion kinetics, lead to the same value of β independently.

This is an evidence that all chlorin e_6 conjugates appear in several species, leading to a distribution of the photosensitizers triplet-state lifetime. This matches to the hypothesis of the albumin interaction.

It was found that the triplet depletion part of the singlet oxygen luminescence kinetics does not follow an exponential decay, leading to a deviation of the singlet oxygen luminescence kinetics from the aforementioned bi-exponential model. A deviation of the singlet oxygen deactivation part of singlet oxygen luminescence kinetics from an exponential decay can only be determined by analyzing the direct time-resolved singlet oxygen luminescence data. The measured kinetics of **4**-**6** can be described by a model containing a mono-exponential singlet oxygen deactivation. However, it appears likely that the photosensitizer's microenvironment is inhomogeneous, but the influence of the inhomogeneity on the singlet oxygen luminescence kinetics is small compared to the influence of the triplet depletion kinetics.

Table 1 lists the singlet oxygen lifetimes and triplet-state lifetimes of the photosensitizers that were obtained in aqueous solution and in cells. Compared to all other chlorins and pheophorbides, chlorin e_6 conjugate **4** in cell suspension is striking with a short singlet oxygen lifetime and a very long triplet-state lifetime.

Photodynamic killing of jurkat cells

The phototoxicity of **1**-**6** was tested *in vitro* on Jurkat cells in suspension. Figure 9 shows the viability of Jurkat cells after incubation with the PEGylated sensitizers. The blank control contained 0.3% ethanol and the sample with mTHPC was used as positive control. None of the samples showed any significant dark toxicity. The PEGylated sensitizers **1**-**6** and mTHPC showed higher phototoxicity compared to dark toxicity.

As a clinical approved photosensitizer, the positive control mTHPC can be considered a "gold standard" in comparison with our PEGylated sensitizers **1**-**6**. The phototoxicity of photosensitizers **2**, **5** and **6** are in the same range or even higher than mTHPC, which corresponds to expectations expressed by measurement of the singlet oxygen generation *in vitro*. The phototoxicities of **1**, **3** and **4** are significantly lower compared to mTHPC. Based on these, phototoxicity experiments **2** and **6** show a maximal effect and low dark toxicity. We note that, due to our illumination of the cells with white light, differences in the absorption spectra of these sensitizers **1**-**6** are expected to be negligible compared to other uncertainties.

Mechanistic summary

Our study of PEGylated photosensitizers **1**-**6** found that:

1 Photosensitizers **1**-**6** are synthesized in good overall percent yields. Pheophorbide-*a* conjugates **1** and **2** were more straightforward to synthesize due to the single attachment of a triPEG galloyl group. Coupling of individual PEG groups in a stepwise fashion to chlorin e_6 was required for **5** and **6**.
2 Our photophysical measurements suggest an interaction of the PEGylated chlorin e_6 conjugates **4**-**6** with albumins. Singlet oxygen luminescence kinetics as well as triplet-state depletion kinetics suggest that the interaction with albumin leads to several different species. There was a noticeable difference in the kinetics of chlorin e_6 conjugate **4** in cells. The different species cannot be distinguished from the data with satisfying numerical certainty.
3 A correlation was found between phototoxicity and the number of PEG groups in **1**-**6**. There was an increase in the Jurkat cell phototoxicity for pheophorbide triPEGylation (**2**) compared to hexaPEGylation (**3**) (24% to 4%, respectively). We attribute this to the hexaPEGylation enhancing solvation and diminishing photosensitizer intercalation into cell membranes. Figure 9 shows that triPEGylation in **2** had enhanced phototoxicity compared to **1,** suggesting that the poor phototoxicity of **1** was due to the carboxylic acid group via reduced intercalation into cell membranes. Chlorin e_6 triPEGylation (**6**) increased the cell phototoxicity compared to monoPEGylation (**4**) from 77% to 4%. Compared to the other PEGylated sensitizers in the series, the monoPEG **4** was the poorest with drawbacks in cell suspension and low phototoxicity.

CONCLUSION

With the completion of the synthesis and *in vitro* evaluation of photosensitizers **1**-**6**, we found that **2** and **6** generate singlet oxygen most efficiently as well as possess highest phototoxicity and lowest dark toxicity to Jurkat cells. The introduction of less or more than 3 PEG groups was clearly less than optimal. In terms of being a test bed for PEG sensitizers, the synthesis of **2** had fewer steps and was higher yielding compared to **6**, but both have favorable photophysical properties for their potential incorporation to fiber tips for PSPDT (Fig. 10). The next objective is to synthetically attach **2** and **6** by their alkene side groups to silica device tips for PSPDT, and the localized killing of head and neck cancer in a mouse tumor model.

Acknowledgements—T.B. thanks the Deutsche Forschungsgemeinschaft (DFG) for funding (RO 1042/33-1). A.A.G. and A.G. acknowledge support from the National Science Foundation (CHE-1464975). A.G. acknowledges support from the Tow Professorship at Brooklyn College. We also thank Leda Lee for the graphic arts work.

SUPPORTING INFORMATION

Additional Supporting Information may be found in the online version of this article:

Figure S1. ^{1}H NMR spectrum of compound **2** in $CDCl_3$.
Figure S2. ^{13}C NMR spectrum of compound **2** in $CDCl_3$.
Figure S3. HSQC spectra of compound **2** in $CDCl_3$.
Figure S4. HMBC spectra of compound **2** in $CDCl_3$.
Figure S5. Expanded HMBC spectra of compound **2.**
Figure S6. COSY spectra of compound **2** in $CDCl_3$.
Figure S7. HPLC spectrum of compound **2.**
Figure S8. ^{1}H NMR spectrum of compound **3** in $CDCl_3$.
Figure S9. ^{13}C NMR spectrum of compound **3** in $CDCl_3$.
Figure S10. HSQC spectra of compound **3** in $CDCl_3$.
Figure S11. HMBC spectra of compound **3** in $CDCl_3$.
Figure S12. Expanded HMBC spectra of compound **3** in $CDCl_3$.

Figure S13. COSY spectra of compound **3** in $CDCl_3$.
Figure S14. HPLC spectrum of compound **3.**
Figure S15. UV-Vis spectra of compounds **1**, **2** and **3.**

REFERENCES

1. Ghogare, A. A., I. Rizvi, T. Hasan and A. Greer (2014) "Point-source" delivery of a photosensitizer drug and singlet oxygen: eradication of glioma cells *in vitro*. *Photochem. Photobiol.* **90**, 1119–1125.
2. Mahendran, A., Y. Kopkalli, G. Ghosh, A. Ghogare, M. Minnis, B. I. Kruft, M. Zamadar, D. Aebisher, L. Davenport and A. Greer (2011) A hand-held fiber-optic implement for the site-specific delivery of photosensitizer and singlet oxygen. *Photochem. Photobiol.* **87**, 1330–1337.
3. Zamadar, M., G. Ghosh, A. Mahendran, M. Minnis, B. I. Kruft, A. Ghogare, D. Aebisher and A. Greer (2011) Photosensitizer drug delivery via an optical fiber. *J. Am. Chem. Soc.* **133**, 7882–7891.
4. Kimani, S., G. Ghosh, A. Ghogare, B. Rudshteyn, D. Bartusik, T. Hasan and A. Greer (2012) Synthesis and characterization of mono-, di-, and tri-poly(ethylene glycol) chlorin e_6 conjugates for the photokilling of human ovarian cancer cells. *J. Org. Chem.* **77**, 10638–10647.
5. Ghogare, A. A. and A. Greer (2016) Synthesis of a poly(ethylene glycol) galloyl sensitizer tip for an 'all-in-one' photodynamic device. *J. Biophotonics* **9**, 1326–1336.
6. Oar, M. A., J. M. Serin, W. R. Dichtel, J. M. J. Fréchet, T. Y. Ohulchanskyy and P. N. Prasad (2005) Photosensitization of singlet oxygen via two-photon-excited fluorescence resonance energy transfer in a water-soluble dendrimer. *Chem. Mater.* **17**, 2267–2275.
7. Hackbarth, S. and B. Röder (2015) Singlet oxygen luminescence kinetics in a heterogeneous environment – identification of the photosensitizer localization in small unilamellar vesicles. *Photochem. Photobiol. Sci.* **14**, 329–334.
8. Schlothauer, J., B. Röder, S. Hackbarth and J. Lademann (2010) In vivo detection of time-resolved singlet oxygen luminescence under Pdt relevant conditions. In *Bios* (Edited by D. H. Kessel), Proc. SPIE7551, Optical Methods for Tumor Treatment and Detection: Mechanisms and Techniques in Photodynamic Therapy XIX, 2010 pp. 755106–755109.
9. Van Stokkum, IHM, D. S. Larsen and R. Van Grondelle (2004) Global and target analysis of time-resolved spectra. *Biochim. Biophys. Acta* **1657**, 82–104.
10. Godfrey, K. (1983) *Compartmental Models and their Application*. Academic Pr, London.
11. Hayek, A., F. Bolze, J.-F. Nicoud, P. L. Nicoud and Y. Baldeck (2006) Synthesis and characterization of water-soluble two-photon excited blue fluorescent chromophores for bioimaging. *Photochem. Photobiol. Sci.* **5**, 102–106.
12. Wang, L.-G., T.-G. Zhan, X. Zhao, X.-K. Jiang and Z.-T. Li (2012) p-Phenyleneethynylene-based comb-like oligomers. *Tetrahedron* **68**, 5303–5310.
13. Maisch, T., J. Baier, B. Franz, M. Maier, M. Landthaler, R.-M. Szeimies and W. Bäumler (2007) The role of singlet oxygen and oxygen concentration in photodynamic inactivation of bacteria. *Proc. Natl. Acad. Sci. USA* **104**, 7223–7228.
14. Jimenez-Banzo, A., X. Ragas, P. Kapusta and S. Nonell (2008) Time-resolved methods in biophysics. 7. Photon counting vs. analog time-resolved singlet oxygen phosphorescence detection. *Photochem. Photobiol. Sci.* **7**, 1003–1010.
15. Egorov, S., V. F. Kamalov, N. I. Koroteev, A. A. Krasnovsky, B. N. Toleutaev and S. V. Zinukov (1989) Rise and decay kinetics of photosensitized singlet oxygen luminescence in water. Measurements with nanosecond time-correlated single photon counting technique. *Chem. Phys. Lett.* **163**, 421–424.
16. Hackbarth, S., T. Bornhütter and B. Röder (2016) Singlet oxygen in heterogeneous systems. *Singlet Oxygen: Appl. Biosci. Nanosci.* **2**, 26.
17. Chen, K., M. Wacker, S. Hackbarth, C. Ludwig, K. Langer and B. Röder (2010) Photophysical evaluation of mTHPC-loaded HSA nanoparticles as novel PDT delivery systems. *J. Photochem. Photobiol., B* **101**, 340–347.
18. Preuss, A., K. Chen, S. Hackbarth, M. Wacker, K. Langer and B. Röder (2011) Photosensitizer loaded HSA nanoparticles II: in vitro investigations. *Int. J. Pharm.* **404**, 308–316.
19. Wacker, M., K. Chen, A. Preuss, K. Possemeyer, B. Röder and K. Langer (2010) Photosensitizer loaded HSA nanoparticles. I: Preparation and photophysical properties. *Int. J. Pharm.* **393**, 253–262.
20. Fanali, G., A. Di Masi, V. Trezza, M. Marino, M. Fasano and P. Ascenzi (2012) Human serum albumin: From bench to bedside. *Mol. Aspects Med.* **33**, 209–290.
21. Cai, H.-H., X. Zhong, P.-H. Yang, W. Wei, J. Chen and J. Cai (2010) Probing site-selective binding of rhodamine B to bovine serum albumin. *Colloids Surf. A* **372**, 35–40.
22. Hess, M., B.-W. Jo, B. Wermeckes, S. Dehne, J.-S. Sohn, S. Wunderlich and M. Zähres (2005) Properties of a water-soluble paclitaxel conjugate in aqueous solution and its interaction with serum albumin. *Macromol. Symp.* **231**, 28–46.
23. Sundaresan, K. V. and R. D. Ludescher (2008) Molecular mobility and oxygen permeability in amorphous β-lactoglobulin films. *Food Hydrocolloids* **22**, 403–413.
24. Borissevitch, I. E., T. T. Tominaga and C. C. Schmitt (1998) Photophysical studies on the interaction of two water-soluble porphyrins with bovine serum albumin. Effects upon the porphyrin triplet state characteristics. *J. Photochem. Photobiol., A* **114**, 201–207.
25. Berberan-Santos, M. N., E. N. Bodunov and B. Valeur (2005) Mathematical functions for the analysis of luminescence decays with underlying distributions 1. Kohlrausch decay function (stretched exponential). *Chem. Phys.* **315**, 171–182.
26. Pollard, H. (1946) The representation of e^{-*x*^{λ}} as a Laplace integral. *Bull. Am. Math. Soc.* **52**, 908–911.
27. Berberan-Santos, M., E. N. Bodunov and B. Valeur (2008) History of the Kohlrausch (stretched exponential) function. *Ann. Phys.* **17**, 460–461.